This document is the Accepted Manuscript version of a Published Work that appeared in final form in [ACS Catalysis], copyright © [2025 American Chemical Society] after peer review and technical editing by the publisher. To access the final edited and published work see [https://pubs.acs.org/articlesonrequest/AOR-SFMIUTXUJPP84DIPXERT].

In situ NMR Spectroscopy and Kinetic Modelling Reveal Pathways and Approaches to Controlling Selectivity in Acid-catalyzed Furfural Oxidation

Stefan S. Warthegau,[1] Ana Jakob,[1,3] Magnus Karlsson,[2] Robert Madsen,[1] Miha Grilc,[3] Pernille Rose Jensen,[2] and Sebastian Meier[1*]

[1] *Department of Chemistry, Technical University of Denmark, Kemitorvet, Building 206, 2800 Kgs Lyngby, Denmark*

[2] *Department of Health Technology, Technical University of Denmark, Elektrovej 349, 2800 Kgs Lyngby, Denmark*

[3] *Department of Catalysis and Chemical Reaction Engineering, National Institute of Chemistry, Hajdrihova 19, 1000 Ljubljana, Slovenia*

KEYWORDS. Biomass upgrading, dDNP NMR, Furanics, In situ NMR, Kinetic modelling, Reaction pathways

ABSTRACT: Furanic compounds have long been known as products that can be formed from carbohydrates in high yields. The need for forming organic precursors and fuels from renewable reactants has hence revitalized the interest in the conversion of furanic precursors to prospective industrial monomers, including acids, diacids, anhydrides and lactones. These precursors can be formed from furfural in oxidative pathways that are catalyzed by Lewis or Brønsted acids. Only recently, strategies to achieve high selectivity to desired products under mild conditions have emerged. These conditions remain discovered by serendipity and screening, as the pathways in the oxidative upgrading of furanics remain poorly understood and controversially discussed. To enable a rational basis for improving the conversions of furanic compounds, we conduct an extensive mechanistic and kinetic study of the oxidation pathways using hydrogen peroxide in Brønsted acidic medium. Specifically, we employ various types of time-resolved *in situ* nuclear magnetic resonance (NMR) spectroscopy to gain insights into pathways, reaction mechanisms, energetics, and kinetics. Spin polarization-enhanced (hyperpolarized) NMR using furfural substrate is used to elucidate the controversial initial steps channeling furfural into the oxidative pathway. With this approach, a reliable kinetic model is derived that accounts for the time course of twelve main chemicals in the reaction cascade towards at least four principal competing products. The approach sheds unprecedented light on the pathways and their control. Divergent steps that decide the product composition are identified through diligent experimentation, and distinct responses to reaction conditions at these branch points are shown to control selectivity for the competing products.

INTRODUCTION

Future society will depend on the sustainable production of organic chemicals as precursors and fuels. To date, the vast majority (95%) of organic chemicals used in the chemical industry remains sourced from fossil fuels.[1–4] The energy and transportation sector is projected to increase to a daily consumption of crude oil of 116 million barrels (18.4 billion liters) per day by 2030.[5] Already today, the global annual fossil emissions surpass 36.8 billion metric tons of carbon dioxide, and the numbers are increasing.[6] Renewable biomass is a potential future resource for both fuels and polyfunctional building blocks. Specifically, carbohydrates can be cheap substrates in pure form and are hence promising renewable substrates for materials and energy demands of the future.[7] Amongst the conversion routes of carbohydrates to other chemicals, the conversion to substituted furans is arguably most widely explored. Such furans include furfural derived from pentoses that are abundant in hemicellulose, and hydroxymethyl furfural derived from hexoses such as glucose, the principal monomer constituent of cellulose. These furanic compounds are promising precursors and platform chemicals that are currently investigated by academic and industrial groups for their use in various applications, including the conversion to polymer building blocks by oxidation or reduction reactions.[8–12] For instance, increasingly benign processes have been identified for the oxidative conversion of furfural to lactones and diacids.[9,13–19] Multifunctional organic acids including the C4 acids maleic acid, fumaric acid and succinic acid may thus be derived from routes to polymer building blocks that do not depend on petrochemicals.[20]

Surprisingly, both the routes for the conversion of carbohydrates to furanics and the routes for the upgrading of furanics to polymer building blocks have remained controversial, although these conversions have been studied since the 19th century.[21,22] The insufficient understanding of these routes impedes the rational development of a carbohydrate-based bioeconomy and optimized reaction conditions remain detected via serendipity. For instance,

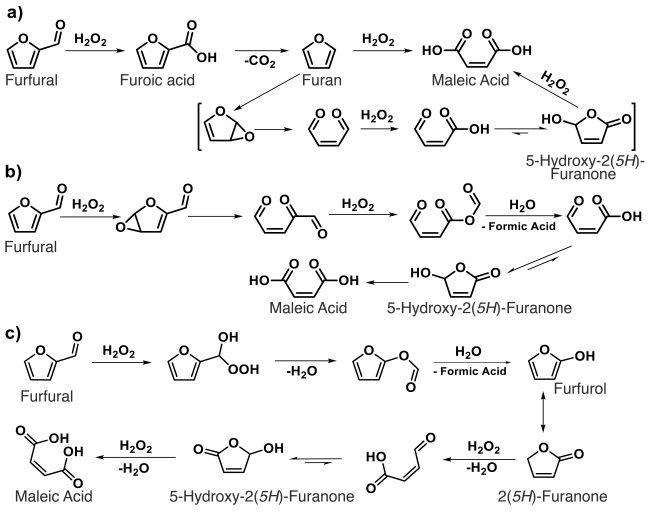

Scheme 1: Previously proposed pathways for the acidic oxidation of furfural: a) oxidation to furoic acid followed by decarboxylation, b) epoxidation followed by ring-opening, c) Baeyer-Villiger oxidation followed by hydrolysis. Adapted from reference 19, available under an ACS AuthorChoice License. Copyright 2020 Y. Lou, S. Marinkovic, B. Estrine, W. Qiang, and G. Enderlin.

the conversion of furfural with hydrogen peroxide in formic acid was described only rather recently as a particularly efficient process for the conversion of furfural to maleic acid under operationally simple and mild conditions.[13] Controversially discussed transformation pathways of furfural in the presence of hydrogen peroxide and acid are compiled in Scheme 1. The plausible pathways can be classified into (i) conversion into furoic acid followed by subsequent decarboxylation (Scheme 1a),[23] (ii) epoxidation of furfural followed by ring-opening (Scheme 1b),[23] and (iii) Baeyer-Villiger oxidation of furfural followed by hydrolysis (Scheme 1c).[14] Each of these pathways culminates in the formation of maleic acid,[19] while other conditions can favor succinic acid or 2(5*H*)-furanone as the primary products (Scheme 1).[10,14,24]

The principal challenge for rational reaction improvement is that short-lived intermediates in chemical reactions often remain difficult to detect and identify.[25,26] This limitation can be especially severe for reaction cascades that proceed via extended pathways entailing several intermediates that are converted spontaneously in subsequent steps. In order to distinguish and identify organic chemicals in ongoing reactions under such conditions, *in situ* Nuclear Magnetic Resonance (NMR) spectroscopy has emerged as a powerful tool for insight into reaction mechanisms, energetics, and kinetics.[27–32] While *in situ* NMR spectroscopy can provide insights into structural conversions and reactivities along complex reaction cascades,[33–36] it has its limitations in detecting and characterizing transient species due to its low sensitivity. These challenges have been recently addressed by dissolution Dynamic Nuclear Polarization NMR (dDNP NMR) spectroscopy, a technique that provides a transformative approach to investigating short-lived substances.[37–40] Initially devised for biomedical imaging, the potential of dDNP NMR has only sporadically been used to gain insight into pathways with relevance to sustainable chemistry.[36,38,41,42] dDNP NMR benefits from the temporary redistribution of nuclear spin states by transferring spin order (*viz.* spin polarization) from electron spins of a doped stable radical species to the nuclear spins of a target substrate by microwave irradiation. In this manner, the sensitivity of NMR measurements can be temporarily enhanced by a factor of 10,000 or more on a seconds to low minutes timescale.[40,43–45] Previous to this study, this approach had not been established for enhancing the sensitivity in furfural probe molecules to examine their conversion.

Here, we explore the kinetics and mechanism of the acid-catalyzed oxidation of furfural with hydrogen peroxide. Complementary timescales for dDNP NMR and conventional NMR were used to clarify the initial controversial steps channeling furfural into the pathways and divergent steps that decide the product composition, respectively. Extensive use of pure intermediates as reaction probes was used to clarify the pathways. A reliable kinetic model was derived that accounts for the time course of twelve main chemicals, which were experimentally observed in the reaction cascade and included previously elusive intermediates. Clarifications of the hitherto controversial mechanisms include direct insight into the formation of transient furan-peroxy adducts before, and furan-esters after, an initial Baeyer-Villiger oxidation. Subsequent branching steps show distinct responses to reaction conditions and control selectivity for the competing products, including unanticipated regimes such as those favoring the formation of the C3 diacid malonic acid. Hence, the results can support improved product control in the upgrading of furanic compounds based on detailed knowledge of branching pathways, their products, and reaction control near the branch points.

MATERIALS AND METHODS

Chemicals. Furfural (99%) and 5-hydroxy-2(5*H*)-furanone were purchased from ThermoScientific (Waltham, MA, USA). The diacids succinic acid (99%), malic acid (95-100%), and malonic acid (99%) were all purchased from Sigma Aldrich (St. Louis, MA, USA), and maleic acid (99%) were purchased from Ferak Berlin GmbH (Berlin, Germany). 2(5*H*)-furanone (98%), furan (98%), and deuterated water (D_2O) were likewise purchased from Sigma Aldrich. Hydrogen peroxide (>30%) and sodium bisulfite were purchased from Fischer Scientific, and formic acid (99-100%) was purchased from VWR. Acetic acid-d_4 (99.5%) was purchased from Cambridge Isotope Lab (Cambridge, UK).

General Reaction Procedures. For a typical *in situ* ^{13}C NMR experiment, the starting material of interest (125-165 µmol) was added to an Eppendorf tube containing 400 µL of a solution of formic acid (10% in demineralized water, (v/v)). From the mixture, 410 µL was added to a 5 mm NMR tube fitted with a D_2O lock tube and a

vented lid to avoid overpressure from the CO_2 produced. Immediately before the start of the NMR experiment, 100 µL of >30% H_2O_2 was added to the NMR tube and the solution was whirlmixed.

For a typical *ex situ* ^{13}C NMR experiment, the starting material of interest (4 mmol) was added to a 25 mL round-bottomed flask fitted with a magnetic stirrer containing 8 mL of a formic acid solution (10% in water (v/v)). To this mixture, 2 mL >30% H_2O_2 was added, and the flask was sealed with a septum fitted with a cannula (to avoid overpressure from the CO_2 produced) and heated in an oil-bath at the desired temperature (typically 40 °C). At given time points, 500 µL of the reaction mixture was withdrawn and transferred to a 5 mm NMR tube fitted with a D_2O lock tube.

NMR Spectroscopy. *In situ* NMR spectra were acquired on an 800 MHz Bruker (Fällanden, Switzerland) Avance III instrument equipped with an 18.7 T magnet and a 5 mm TCI cryoprobe. The time-resolved reaction tracking was conducted by implementing a time series of 1D ^{13}C NMR spectra (zgig30) as a pseudo-2D experiment. An inter-scan relaxation delay d1 of 1.5 s was used, and 200–512 transients of the FID were accumulated, subject to the sensitivity required. The FID was sampled during an acquisition time of 0.68 s. ^{1}H-^{13}C HSQC, ^{1}H-^{13}C HMBC, and ^{1}H-^{1}H TOCSY were employed for structure determination and chemical shift assignments. *Ex situ* 1D ^{13}C NMR Spectra were acquired on a 400 MHz Bruker Avance III HD NMR instrument equipped with an Ascend magnet and a BBO Prodigy probe. All spectra were acquired and processed using Bruker Topspin 3.5 pl6 and analyzed using Bruker Topspin 3.5 pl6 or 4.3.0. Integrals of signals for the detected species were extracted from pseudo-2D experiments using the Dynamics module of the same software. Minor fluctuations in the overall carbon balance in all experiments were observed (5-15% deviation) due to non-complete inter-scan relaxation during data accumulation. Hence, the overall carbon signal during the reaction was normalized prior to fitting, to honor mass conservation and reduce errors imparted by the relaxation behavior of the observed chemicals. No discoloration or polymerization was observed in the samples.

dDNP NMR Spectroscopy. A substrate sample stock solution was prepared from a mixture of furfural at natural isotope abundance (150 µL, 174 mg, 1.82 mmol) and PEG 400 (150 µL, 169.5 mg), which was doped with trityl radical AH111501 (GE Healthcare, M_w = 1595 g/mol, 16.8 mg for 35 mM). 115 mg of the furfural/PEG400/radical solution was hyperpolarized in a Spin-Aligner 6.7 T polarizer (Polarize ApS). After build-up of hyperpolarization for 1 hour, the sample was dissolved in 5 ml MilliQ water. The concentration of furfural after dissolution was 121 mM. The dissolved hyperpolarized furfural was collected in a 50 mL receiver container at the polarizer and 1 mL was drawn into a 1 mL syringe. This hyperpolarized substrate solution was rapidly transferred to the NMR magnet, where the hyperpolarized solution was manually injected into the NMR tube via an inlet line (with 700 µL of void volume). For reaction tracking on the seconds time scale, 300 µL hyperpolarized solution was injected into a mixture of 240 µL formic acid (50% in water (v/v)) and 60 µL hydrogen peroxide (>30% in water (v/v)) residing in the NMR instrument at 37 °C, resulting in a final temperature near 40 °C upon injection of furfural dissolved in hot buffer. NMR spectra were recorded as a time series of ^{13}C spectra implemented as a pseudo-2D experiment on a Bruker 500 MHz AVANCE NEO spectrometer equipped with a 5 mm DCH cryoprobe. After injection of the hyperpolarized furfural, the time series of ^{13}C NMR spectra was recorded using a nominal pulse angle of 10° and 1.5 s time resolution.

Kinetic Model Fitting. The reaction scheme developed for kinetic modeling encompassed twelve molecular species, including only detectable products and intermediates. Due to the large surplus of hydrogen peroxide and formic acid, all reaction steps were considered pseudo-first order. Consequently, the rate (r_i) of each reaction was assumed to solely depend on the respective rate constant (k) and reactant concentration (C), as shown in Equation 1. Signals from the ^{13}C NMR experiment were converted to molar concentrations.

(1) $r_\mathrm{i} = k_\mathrm{i} C_\mathrm{j}$

The general molar (n) balance in the solution volume (V) can be described with Equation 2, while the differential equations of each individual compound (j) can be found in the Supplementary Information.

(2) $\frac{1}{V}\frac{dn_\mathrm{j}}{dt} = \frac{dC_\mathrm{j}}{dt} = \sum_\mathrm{i}^\mathrm{I} \pm r_\mathrm{i}$

The set of ordinary differential equations representing molar balances were solved using the Runge-Kutta 2-3 algorithm in Matlab 2018 to predict concentration profiles over time.

The reaction rate constants were estimated by regression analysis, where profiles of time-dependent concentrations derived from ^{13}C NMR integrals were fitted, hence minimizing the objective function (Equation 3 below) using Nelder Mead method.

(3) $\left(k_\mathrm{i-j}\right) = \sum_{exp=1}^{EXP} \sum_{j=1}^{J} \left(C_{exp} - C_{mod}\left(k_{i-j}\right)\right)^2$

Experimental Procedure for the Synthesis of 2(3*H*)-Furanone. To a 250 mL round-bottom flask fitted with a magnetic stirrer furfural (5.0 mL, 60.36 mmol, 1.0 equiv.) and formic acid (10% in H_2O (v/v), 120 mL, 318.19 mmol, 5.3 equiv.) were added, and the mixture was mixed until homogenized. Hydrogen peroxide (>30% in H_2O, 30 mL, 293.70 mmol, 4.9 equiv.) was added to the mixture, and the resulting solution was stirred at 40 °C in an oil bath. After 45 minutes, the solution was cooled to room temperature, extracted three times with dichloromethane (3×40 mL), the combined organic layers

dried with anhydrous $MgSO_4$, filtered, and volatiles removed *in vacuo*. This work-up resulted in 5.4 g of a mixture of furfural and 2(3*H*)-furanone (~3:1 furfural/2(3*H*)-furanone). Next, acetone (10 mL) was added to the mixture, and the solution was poured into a 100 mL separatory funnel. A saturated sodium bisulfite solution (20 mL) and dichloromethane (20 mL) were added to the separatory funnel. Upon shaking, addition of water (20 mL) and further shaking, the phases separated well and were collected. Saturated sodium bisulfite solution (20 mL) was added to the organic layer. Upon shaking, addition of water (20 mL) and further shaking, the separate layers were collected. The organic layer was extracted with water (20 mL) to remove any remaining sodium bisulfite, prior to drying with anhydrous $MgSO_4$, filtration, and removal of the volatiles *in vacuo*, to yield 2(3*H*)-furanone (**3**). Purified 2(3*H*)-furanone (**3**) was found to spontaneously isomerize to 2(5*H*)-furanone (**4**) at room temperature on a time scale of days. Due to its spontaneous isomerization to 2(5*H*)-furanone (**4**), 2(3*H*)-furanone (**3**) was used as a substrate directly after purification and was stored at -18 °C for improved shelf-life.

RESULTS AND DISCUSSION

Suitable reaction conditions and assignments of molecular species using *ex situ* NMR. A wide range of homogeneous and heterogeneous acids were previously used to catalyze the conversion of furfural in the presence of oxidant. Due to their operational simplicity, we followed approaches using reaction media encompassing aqueous hydrogen peroxide as the oxidant and homogeneous Brønsted acids as catalysts. Specifically, the combined use of formic acid and hydrogen peroxide was rather recently described as an operationally simple promising medium for the quantitative and selective oxidation of furfural to maleic acid.[13] We hence set out to determine the principally accessible pathways in the formic acid-catalyzed oxidation of furfural as an initial step towards controlling activity and selectivity in the pathway. To this end, we chose to employ *in situ* ^{13}C NMR spectroscopy in addition to multidimensional and hyperpolarized NMR for a time-resolved tracking of the reaction pathways.

Initially, we identified mild reaction conditions that afforded full furfural conversion within 3 hours. We conducted a time series of conversions using approximately 5 equivalents of formic acid and hydrogen peroxide relative to furfural (0.5 M) at 40 °C in an oil bath under stirring. One-dimensional ^{13}C NMR spectra were acquired at discrete time points (Figure 1), where the deshielded olefinic and oxidized carbons are shown as structural reporters of twelve main chemicals. These signals were assigned to the chemical structures shown in Figure 1 by rapidly subjecting the samples to high-field heteronuclear assignment spectra including ^{1}H-^{13}C HSQC and ^{1}H-^{13}C HMBC spectra. Careful experimentation and analysis allowed the distinction of hydrates and hydroperoxy adducts of the aldehyde groups present in the substrate and in some of the emerging intermediate species. Furfural was found to rapidly form a hydroperoxy adduct (63% relative to furfural, Figure S1), while no significant amounts of a hydrate form were found. The formation of hydroperoxy adducts over hydrates can be explained by the α-effect: increased nucleophilicity and reactivity of hydrogen peroxide oxygen relative to water results from the adjacent lone-pair-bearing atom in hydrogen peroxide.[46] The spectral assignments that were derived from the *ex situ* samples with the described approach are compiled in Figure 2 for the twelve molecular species **1**–**12**. These compounds encompass 2(3*H*)-furanone (**3**), succinic acid (**7**), malic acid (**9**), and malonic acid (**11**) in addition to the hydroperoxide adducts of their semialdehydes (**6, 8,** and **10,** respectively), which have not been previously observed as pathway intermediates. NMR identifications of the peroxy adducts relative to hydrate forms in compounds **8** and **10** followed the loss of symmetry at the aldehyde groups. Addition of hydroperoxide to the aldehyde group results in the formation of a stereogenic center at this group. Hydroperoxy adducts could hence be identified by the presence of signal doubling from diastereomeric forms of chemical **8** containing an additional stereogenic center, and by non-equivalence of diastereotopic methylene protons in **6** (Figure S2), while these protons would be enantiotopic and hence chemically equivalent in the hydrate. All assignments were consistent with computational predictions of ^{1}H and ^{13}C chemical shifts and with published experimental chemical shifts values, for the instances where published data were available. Overall, *ex situ* NMR on furfural oxidation in a formic acid/hydrogen peroxide medium at mild temperatures afforded

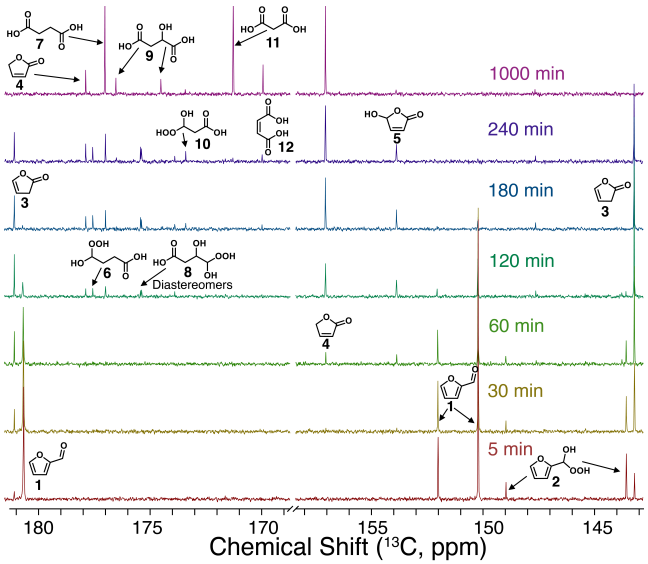

Figure 1. ^{13}C-NMR spectra (D_2O lock tube, 25 °C) of furfural oxidation under stirring. Olefinic and oxidized carbons are shown as structural reporter groups of the displayed structures. The formic acid region is omitted for clarity. Reaction conditions: Furfural (333 µL, 4.02 mmol, 1 equiv.), hydrogen peroxide (>30%, 2.0 mL, 19.58 mmol, 4.9 equiv.), and formic acid (10% in H_2O, 8 mL, 21.21 mmol, 5.3 equiv.) at 40 °C under stirring.

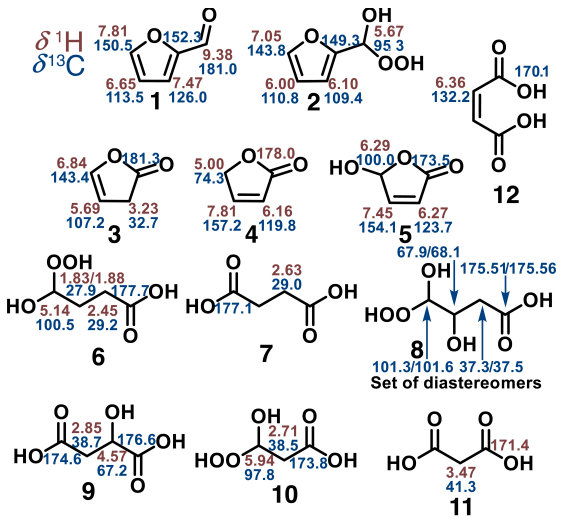

Figure 2. Full chemical shift assignments of ^{13}C and non-labile ^{1}H for compounds observed in the acidic oxidation of furfural. All assignments are consistent with computational predictions and with published values, where available.

the detection and identification of previously elusive intermediates and indicated that a diverse set of products, including four dicarboxylic acid products, can be formed in competing pathways. Hence, the reaction pathways that were accessible in the conversion of furfural in formic acid/hydrogen peroxide medium were more complex than initially anticipated.

***In situ* NMR to clarify the temporal succession of the detected species.** To gain insight into the sequential steps of furfural oxidation pathways, we undertook to establish an *in situ* reaction system. The *in situ* reaction systems contained minor modifications to the *ex situ* reaction system, as the absence of stirring in the NMR sample tube led to slower transformations, as expected.[47] We hence found that an increase in formic acid and hydrogen

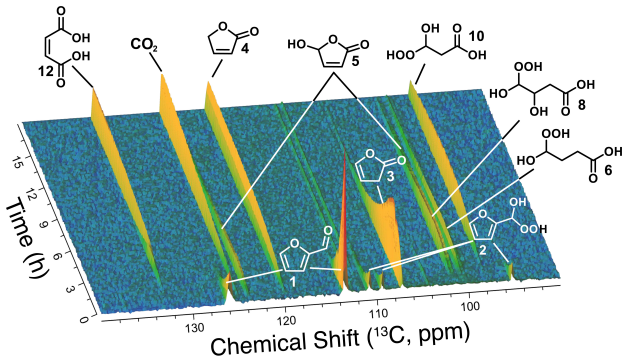

Figure 3. Time series of *in situ* ^{13}C-NMR spectra (201 MHz, D_2O lock tube, 40 °C) in an ongoing reaction of a mixture of furfural (10.4 µL, 124.8 µmol, 1 equiv.), hydrogen peroxide (>30%, 100 µL, 979.0 µmol, 7.8 equiv.), and formic acid (10% in H_2O, 400 µL, 1.06 mmol, 8.5 equiv.) showing the conversion of furfural to several intermediates and products. A reference experiment in the absence of furfural showed that CO_2 derived from the oxidation of formic acid to carbonic acid.

peroxide concentrations (to 8 equiv. relative to furfural) was beneficial to ensure full conversion of furfural within few hours of reaction time and to provide sufficient conversion of furfural along its viable conversion pathways. The conversion of furfural was tracked by acquiring a series of 1D ^{13}C NMR spectra with a time resolution of 10 minutes (Figure 3). Reactions were followed on an 800 MHz NMR instrument equipped with a TCI cryoprobe to provide sufficient sensitivity for accurate quantification of chemicals along the transformation pathway and for the detection of transient species that accumulate to approximately 2 mM or more along the reaction pathway. Spectra were acquired with inverse gated decoupling to allow a reliable conversion of signal areas to molar concentrations.

The *in situ* observation of furfural oxidation in formic acid/hydrogen peroxide medium further corroborated the structural identifications of Figure 2: identical time-courses for the different carbon atoms in a specific molecular species validated their assignment to the same molecule. In this manner, time-dependent reaction progress data for compounds **1**–**12** were obtained using *in situ* ^{13}C NMR spectroscopy in a sensitive experimental setup, and progress data could be converted to molar concentrations.

Despite the complexity in the molecular pathways of furfural conversion observed using both *ex situ* and *in situ* NMR data, the observed species aligned best with the pathway of Scheme 1c, as compound **4** is unique to this pathway among the simplified pathways shown in Scheme 1. We however noted that despite the optimization of the reaction scheme and the use of high-field NMR instrumentation with cryogenically cooled detection electronics, plausible intermediates of the pathway shown Scheme 1c were not directly detectable. This pathway channels furfural into the oxidative pathway through an initial Baeyer-Villiger oxidation. The formyl ester of furfural (**2a**), 2-furanol (**3a**), and *cis*-β-formylacrylic acid (**5a**) were not detected using conventional *in situ* ^{13}C NMR. Their absence suggested that these species were inherently short-lived under these reaction conditions. This is unsurprising for 2-furanol (**3a**) and *cis*-β-formylacrylic acid (**5a**), as previous reports have indicated their increased stability in isomeric forms 2(3*H*)-furanone (**3**) and 5-hydroxy-2(5*H*)-furanone (**5**), respectively.[19,48] By contrast, the absence of the formyl ester of furfural (**2a**) can be rationalized, as acidic aqueous conditions were conducive to fast hydrolysis and to obstructing the accumulation of the formyl ester of furfural to sufficient concentrations for detection.

These considerations would overall suggest that the liberation of formic acid from the formyl ester of furfural (**2a**) and the concurrent formation of 2-furanol, which rapidly tautomerizes to 2(3*H*)-furanone (**3**), result in the concurrent formation of formic acid and **3**. In order to support these considerations, an *in situ* experiment was

conducted in acetic acid-d_4 to observe the formation of formic acid during the reaction and compare it to the formation of 2(3*H*)-furanone (**3**). The formation of formic acid as one of the initial products of furfural oxidation was indeed feasible in this manner. In addition, the resultant time-course data were indeed consistent with an initial concurrent formation of formic acid and (**3**) (Figure 4). This outcome indirectly substantiated the initial formation and hydrolysis of the formyl ester of furfural.

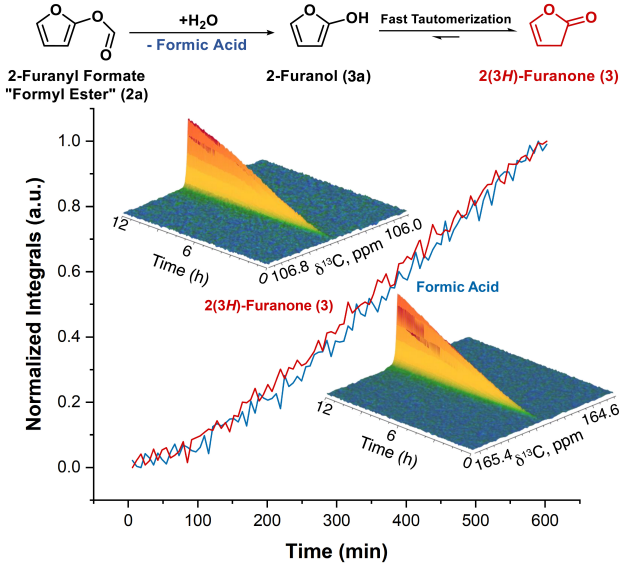

Figure 4. Reaction process curves of 2(3*H*)-furanone (red) and formic acid (blue), displaying their concurrent and similar formation. Reaction conductions: Furfural (10.4 µL, 124.8 µmol, 1 equiv.), hydrogen peroxide (>30%, 100 µL, 979.0 µmol, 7.8 equiv.), and acetic acid-d_4 (10% in H_2O, 400 µL, 1.06 mmol, 8.5 equiv.), 40 °C.

dDNP NMR supports initial Baeyer-Villiger oxidation. Considering persistent controversial opinions about the earliest stages of furfural influx into oxidative pathways, we then chose to probe the initial steps of the pathway using hyperpolarized NMR spectroscopy. To this end, a hyperpolarization protocol was established that allowed the enhancement of furfural ^{13}C nuclear spin polarization by more than a factor of 10,000 using an approach known as dissolution dynamic nuclear polarization (dDNP). In this manner, furfural could be produced as a spin polarization-enhanced tracer in a dedicated polarizer (6.7 T magnet) by microwave-driven transfer of polarization from an electron dopant to furfural in a frozen glass.[45] Upon washing furfural out of the polarizer with hot solvent, the hyperpolarized furfural was forcefully injected into a reaction medium residing in an NMR spectrometer equipped with cryogenically cooled detection electronics. This approach allowed the conversion of furfural to be monitored on a seconds to low minutes time scale to visualize the initial steps in its conversion by dDNP NMR.

The dDNP NMR experiment was conducted with various reaction media to clarify the species that were observed in the experiment (Figure 5). The hyperpolarized furfural was injected into water and into water containing formic acid, both of which resulted in identical spectra containing signals from furfural without indication of its conversion. The experiment was repeated with hydrogen peroxide in water as a reaction medium, resulting in the formation of the hydroperoxy adduct **2**. Only the combined presence of formic acid and hydrogen peroxide in aqueous reaction medium afforded the formation of an unknown species that emerged after the formation of the hydroperoxy adduct **2**. This signal appeared at a ^{13}C chemical shift of 159.6 ppm (Figure 5) and the nature of the dDNP NMR experiment using furfural as the hyperpolarized substrate dictates that the carbon signal derives from hyperpolarized furfural. Comparison to the assigned chemical shift values in species **1**–**12** showed that this molecular species does not represent any of the molecules **1**–**12**. This signal most plausibly originates from the formate-carbon of the formyl ester of furanol (**2a**), whose chemical shift was predicted with a stereochemically and conformationally aware deep learning calculator[49] to 158.5 ppm. In addition to the hydroperoxy adduct of furfural and the formyl ester of furanol, the dDNP NMR experiment further detected the subsequent formation of 2(3*H*)-furanone (**3**).

Overall, the *in situ* NMR experiment employing acetic acid-d_4 and the dDNP NMR experiment using vastly spin polarization-enhanced furfural substrate provide indirect and direct evidence of the conversion of furfural through a Baeyer-Villiger oxidation to the rapidly hydrolyzed formyl ester of furanol, resulting in the formation of 2(3*H*)-furanone (**3**) upon tautomerization of furanol.

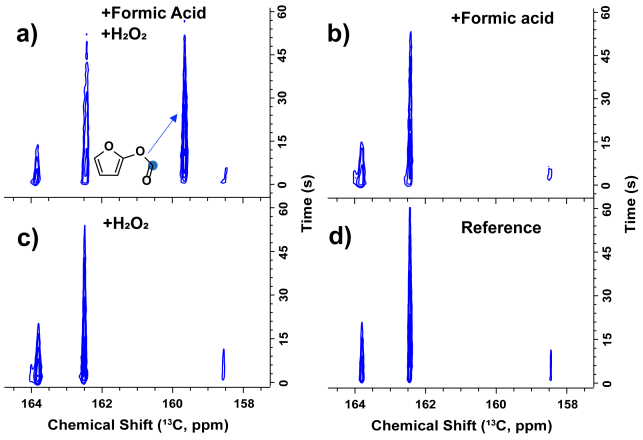

Figure 5. dDNP NMR experiments of hyperpolarized furfural in formic acid and hydrogen peroxide (a), in the absence of hydrogen peroxide (b), in the absence of formic acid (c), and in water (d), showcasing the appearance of an unknown signal at 159.6 ppm, potentially originating from the formyl ester of furfural. Reaction conditions: 300 µL hyperpolarized furfural solution injected into a solution of 240 µL 50% formic acid or water, and 60 µL 30% H_2O_2 at approximately 40 °C.

Use of various substrates to clarify the provenance of compounds. Key intermediates in the *ex situ* and *in situ* reaction tracking of furfural oxidation in a formic acid/hydrogen peroxide medium included the furanones 2(3*H*)-furanone (**3**), 2(5*H*)-furanone (**4**) and 5-hydroxy-

2(5*H*)-furanone (**5**). These furanones have previously been suggested as promising precursors that can be obtained from furfural with close to stochiometric amounts of oxidants.[9,50] While 2(3*H*)-furanone (**3**) and 5-hydroxy-2(5*H*)-furanone (**5**) were intermediates that were converted with surplus hydrogen peroxide in our reactions, 2(5*H*)-furanone (**4**) was considerably more stable in our *ex situ* and *in situ* reactions, to a degree that it could be characterized as a side product to the diacids even in the presence of 8 equiv. hydrogen peroxide.

Considering their different stability in the complex reaction medium, we undertook to explore the reactivity of furanones 2(3*H*)-furanone (**3**), 2(5*H*)-furanone (**4**) and 5-hydroxy-2(5*H*)-furanone (**5**) as authentic substrates to clarify some routes in the oxidative conversion of furfural in a divide-and-conquer approach. Subjecting 2(5*H*)-furanone (**4**) to formic acid/hydrogen peroxide medium at 40 °C did not yield further conversion, and further conversion was not even observed when increasing the temperature to 60 °C and the concentration of formic acid in the solution to 77% (by employing 99% formic acid).

Opposite to the stable 2(5*H*)-furanone (**4**), 2(3*H*)-furanone (**3**) was not easily commercially available. We hence established a purification protocol for 2(3*H*)-furanone (**3**) from the conversion of furfural in formic acid/hydrogen peroxide medium at 40 °C, as 2(3*H*)-furanone (**3**) is a strongly accumulating intermediate under the given reaction conditions. The reaction mixture was allowed to react for 45 minutes, and only 2(3*H*)-furanone (**3**) and furfural (**1**) were present in considerable amounts after reaction workup, in addition to traces of 2(5*H*)-furanone (**4**) (Figure S3). Isolating 2(3*H*)-furanone (**3**) from furfural (**1**) posed challenges due to similar boiling points and R_f-values. Isolation was hence achieved through liquid-liquid extraction using saturated sodium bisulfite.[51] An *in situ* experiment was conducted with the isolated 2(3*H*)-furanone (**3**) at conditions resembling those of the furfural oxidation (Figure 6). The transformation showed the unsurprising formation of succinic

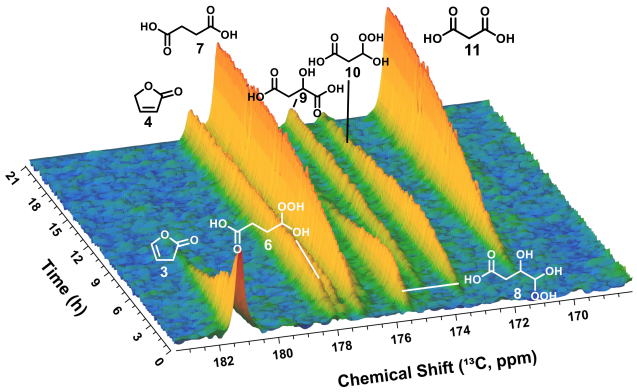

Figure 6. Time series of *in situ* ^{13}C-NMR spectra (201 MHz, D_2O lock tube, 25 °C) of a mixture of 2(3*H*)-furanone (10.0 µL, 140.3 µmol, 1 equiv.), hydrogen peroxide (>30% in H_2O, 100 µL, 979.0 µmol, 7.0 equiv.), and formic acid (10% in H_2O, 400 µL, 1.06 mmol, 7.6 equiv.).

acid (**7**) and the hydroperoxy adduct of its semialdehyde (**6**), but also the formation of both malic acid (**9**), malonic acid (**11**), and the hydroperoxide adduct of their semialdehydes, **8** and **10**, respectively, as well as the formation of 2(5*H*)-furanone (**4**). By contrast, little to no formation of either 5-hydroxy-2(5*H*)-furanone (**5**) or maleic acid (**12**) was observed. These observations suggested that the formation of 5-hydroxy-2(5*H*)-furanone (**5**), and subsequently of maleic acid (**12**), occurred in competition with the formation of furanones **3** or **4**.

Finally, the use of 5-hydroxy-2(5*H*)-furanone (**5**) as the substrate yielded its conversion to maleic acid with high selectivity, while 2(3*H*)-furanone (**3**), 2(5*H*)-furanone (**4**) and diacids beyond maleic acid were not observed (Figure S4). It was surprising that the reaction starting from (**5**) did not yield malic acid (**9**). Intuitively, malic acid (**9**) could be a direct product of maleic acid hydration (**12**) in acidic environments. However, the experiment surprisingly validated that malic acid (**9**) originated from a different pathway. Finally, the diacids succinic acid, malic acid, malonic acid, and maleic acid (**7**, **9**, **11** and **12**) were subjected to the standard reaction conditions in formic acid/hydrogen peroxide medium, which led to no conversion. This observation showed that these diacids were stable under the standard reaction conditions and constituted end products of different routes of furfural oxidation.

For completeness, we finally subjected furoic acid to our standard reaction conditions in formic acid/hydrogen peroxide medium. Furoic acid did not show any signs of

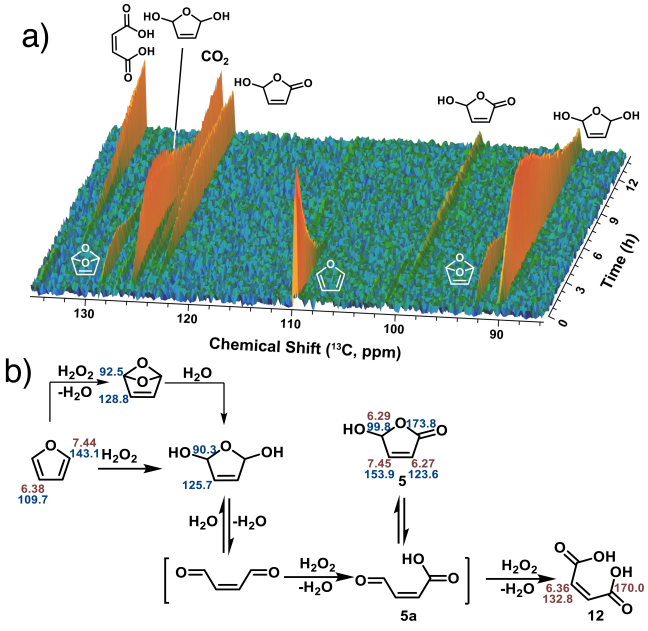

Figure 7. (a) Time series of *in situ* ^{13}C-NMR spectra (201 MHz, D_2O lock tube, 25 °C) in an ongoing reaction of a mixture of furan (12 µL, 165.0 µmol, 1 equiv.), hydrogen peroxide (>30% in H_2O, 100 µL, 979.0 µmol, 5.9 equiv.), and formic acid (10% in H_2O, 400 µL, 1.06 mmol, 6.4 equiv.). The reaction was conducted at room temperature due to the low boiling point of furan. (b) Plausible reaction pathway.

rapid decarboxylation to furan and CO_2, thus excluding a significant contribution of a pathway resembling Scheme 1a with initial furfural oxidation to furoic acid. Instead, furan was used as the starting material to track its conversion, as several sources have claimed that furan converts into maleic acid almost quantitatively (Figure 7).[13,52]

Early stages of the reaction with furan were notably different from the furfural oxidation, yielding both an epoxidation product and 2,5-dihydroxy-2,5-dihydrofuran, which were not observed in the conversion of furfural. However, the pathway converges with parts of the furfural conversion pathway, as both 5-hydroxy-2(5*H*)-furanone (**5**) and maleic acid (**12**) were observed. These observations further validated that maleic acid originated from 5-hydroxy-2(5*H*)-furanone (**5**). Interestingly, the reaction products formed from furan resembled the products formed from 5-hydroxy-2(5*H*)-furanone (**5**) as the starting material. As for the reaction commencing from (**5**), the conversion of furan yielded maleic acid as the predominant product, but did not yield malic acid (**9**), as no hydration of maleic acid to malic acid occurred at significant amounts. Overall, the NMR analysis of reactions starting from commercial or purified chemicals that occur as intermediates in the furfural conversion yielded the conversions depicted in Scheme 2.

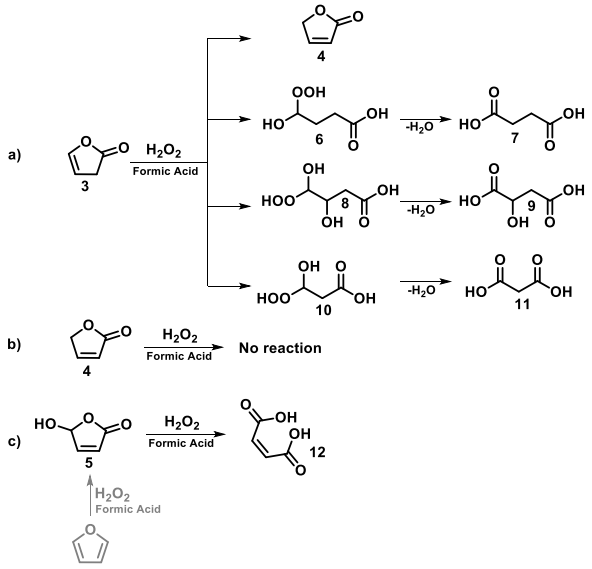

Scheme 2. Reactions with the furanones **3** (a), **4** (b), and **5** (c), showcasing their conversion to different products indicating bifurcation in the acidic oxidation of furfural. Reaction conditions: 140 µmol furanone, 100 µL >30% H_2O_2, and 400 µL 10% formic acid solution, 40 °C.

Plausible mechanism for the acidic oxidation of furfural. The detection of early intermediates with hyperpolarized NMR and the discovery of the bifurcating reaction mechanism from various staring materials were incorporated into a plausible mechanistic model for the acidic oxidation of furfural based on direct real-time observations (Scheme 3). This proposed mechanism resembles initial expectations only in some regards. For instance, the formation of succinic acid (**7**) from 2(3*H*)-furanone (**3**) in a weakly acidic environment and the formation of maleic acid from 5-hydroxy-2(5*H*)-furanone (**5**) were expected from previous studies. By contrast, the observation of hydroperoxide adducts of the semialdehydes of the diacids (**6**, **8**, and **10**) as intermediates, albeit intuitively expected, was not previously reported. Additionally, it was unexpectedly found that malic acid (**9**) derived from 2(3*H*)-furanone (**3**), rather than from the anticipated addition of water to either the double bond in hydroperoxy maleic semialdehyde (**5b**) or maleic acid (**12**). Instead, we propose that performic acid (which is formed from the equilibrium between formic acid and hydrogen peroxide) epoxidates the double bond in 2(3*H*)-furanone (**3**) followed by rapid hydrolysis to form malic semialdehyde and subsequent hydroperoxide addition to form **8**, hence resembling the formation of the other diacids. Less focus has been given to the formation of malonic acid (**11**) in the literature,[20] making its significant appearance among the products within the reaction mixture surprising. The loss of an extra carbon in the formation of this C3 compound is plausibly achieved by a Baeyer-Villiger oxidation resembling the initial conversion of furfural. We hence propose that **10** originates from a Baeyer-Villiger oxidation of the hydroperoxy adduct of malic semialdehyde (**8**). Plausible arrow-mechanisms for the formation of maleic acid (**12**), succinic acid (**7**), malic acid (**9**), and malonic acid (**11**) are compiled in Scheme S1.

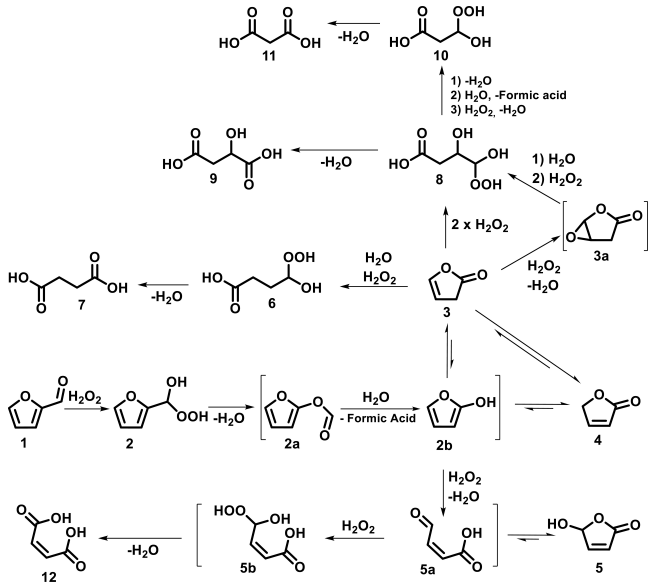

Scheme 3. Plausible mechanism for the formic acid-mediated oxidation of furfural (**1**) based on real-time observations.

Kinetic fitting supports the proposed reaction mechanism. To probe the plausibility of the proposed reaction pathways, kinetic fitting of time-dependent concentration profiles to the proposed branching pathways was performed. Concentration profiles were obtained

from the *in situ* ^{13}C NMR data. The kinetic fitting was based on the simplified reaction mechanism shown in Figure 8e, which only includes concentration data of the twelve quantified species. These determinations were based on the experiments shown in Figure 2, Figure 6, and Figure S4. The experimental data and fitted data plots are compiled in Figure 8. The resulting fitted data on the twelve observed chemicals (**1**–**12**) were in excellent agreement with the experimental data. Given the complexity of the various conversion pathways, this consistency arguably supports the proposed mechanism. Some minor issues remain with the treatment of the early intermediates **2** and **3**, as these were transformed into the largest number of products (Scheme 3). Notwithstanding, the excellent fits obtained when employing 2(3*H*)-furanone and 5-hydroxy-2(5*H*)-furanone as the starting materials (Figures 8b+c and 8d, respectively) confirm the plausibility of the later stages of the reaction that determine the composition of products. The fitting further rationalizes the distribution of the diacids downstream of branch points by kinetic control of competing reactions. Generally, all fitted rate constants were within a reasonable range without outliers (Figure 8e). Hence, there was consistency between experimental data, fitting method and kinetic model, which considered twelve experimentally observed species (**1**–**12**) whose conversion pathways were probed using pure intermediates and polarization enhanced furfural. Thus, this model incorporates an extensive set of reactions including new intermediates and should facilitate more accurate predictions of reaction outcomes relative to previous models.

Intensification and rational improvement of furfural oxidation by acid/H_2O_2. We hence finally attempted to rationalize reaction control based on the mechanistic model of Scheme 3. To this end, we intensified the reaction conditions and chose reaction conditions that were implicated with high selectivity towards the formation of maleic acid. These conditions included the use of more harsh conditions with respect to acid, oxidant, and temperature. Specifically, the use of 100% formic acid, 30% hydrogen peroxide, and 60 °C was reported to provide high selectivity towards maleic acid.[13] We therefore used these conditions to validate previous reports in our setup. The conditions indeed led to vigorous reactions that prevented the observation of the short-lived intermediates crucial for elucidating the precise reaction mechanism using *in situ* NMR. Within 30 minutes of reaction time, maleic acid (**12**) emerged as the primary product (79%), alongside 2(5*H*)-furanone (**4**) and 5-hydroxy-2(5*H*)-furanone (**5**) as byproducts (6% and 15%, respectively).

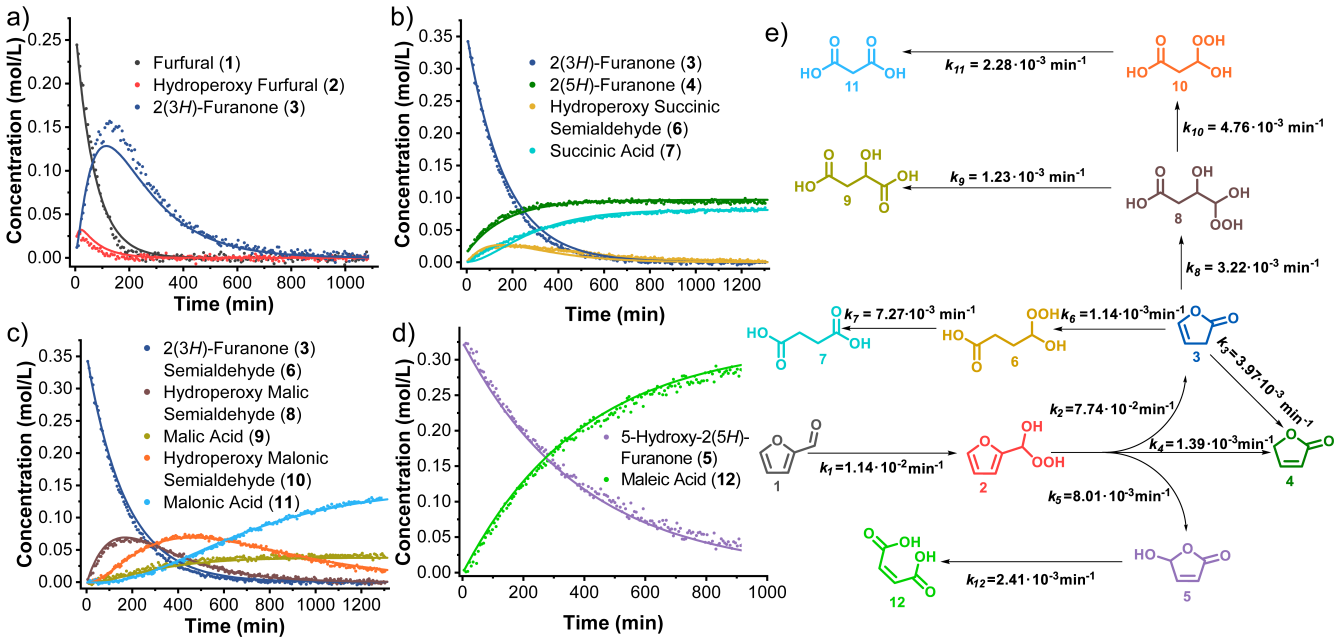

Figure 8. Experimental (●) and fitted (—) data plots of furfural (●), hydroperoxy furfural (●), 2(3*H*)-furanone (●), 2(5*H*)-furanone (●), 5-hydroxy-2(5*H*)-furanone (●), hydroperoxy adduct of succinic semialdehyde (●), succinic acid (●), hydroperoxy adduct of malic semialdehyde (●), malic acid (●), hydroperoxy adduct of malonic semialdehyde (●), malonic acid (●), and maleic acid (●) based on (a) the furfural oxidation experiment in Figure 3, (b,c) the 2(3*H*)-furanone oxidation experiment in Figure 6, (d) the 5-hydroxy-2(5*H*)-furanone oxidation in Figure S4. The full set of integrals for experiments (a-d) is shown alongside fits in Figure S5. (e) Simplified reaction mechanism of the oxidation of furfural with calculated and fitted rate constants, including time-dependent concentration measurements of the compounds observed using in situ NMR experiments.

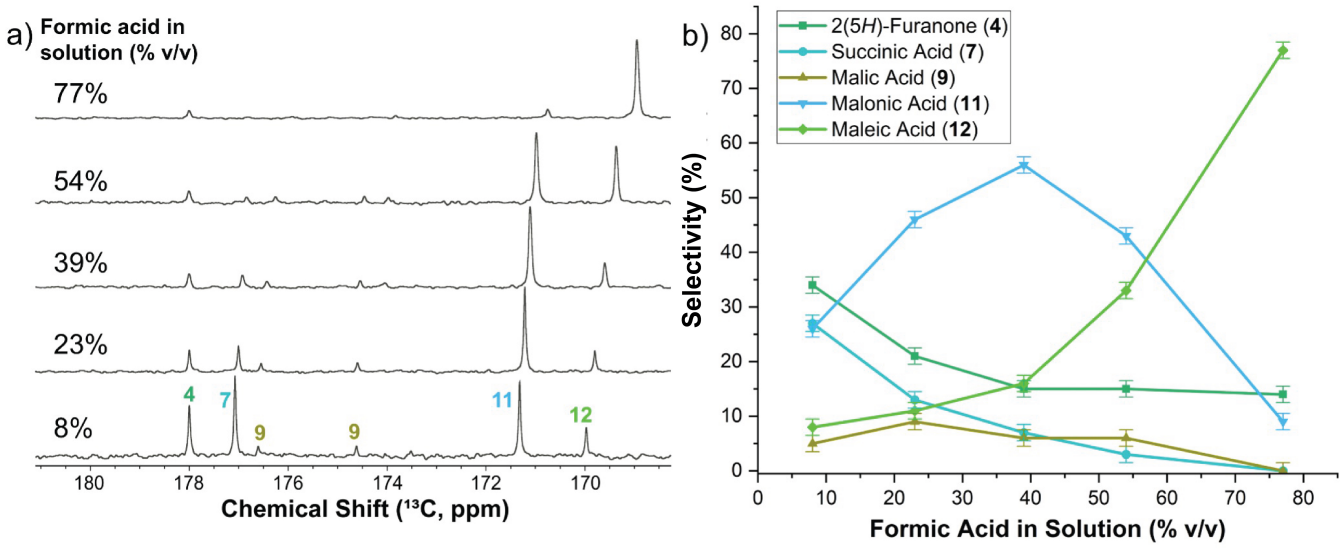

Figure 9. (a) 1D ^{13}C NMR spectra for end point experiments showing product distributions at different concentrations of formic acid in the acidic oxidation of furfural, employing concentrations of 10% formic acid (giving the total concentration of acid in solution the to be 8% v/v), 30% formic acid (23%), 50% formic acid (39%), 70% formic acid (54%), and 100% formic acid (77%). Conditions: furfural (33 µL, 402 µmol), formic acid (800 µL, either 10%, 30%, 50%, 70%, or 100%), and hydrogen peroxide (>30%, 200 µL, 212 µmol), 40 °C, 24 h. (b) Product distribution after 24 hours for different concentrations of formic acid.

The presence of 2(5*H*)-furanone (**4**) indicated that the mechanism of Scheme 1 towards maleic acid was still valid. However, the conversion of the Baeyer-Villiger oxidation products to 5-hydroxy-2(5*H*)-furanone (**5**) seem vastly increased under harsh conditions (100% formic acid, 30% hydrogen peroxide, 60 °C) relative to lower Brønsted acid and oxidant concentration as well as temperature. Thus, tautomerization of the transiently formed furanol to 2(3*H*)-furanone (**3**) and 2(5*H*)-furanone (**4**) evidently is less pH-dependent than the oxidation to 5-hydroxy-2(5*H*)-furanone (**5**). This observation was consistent with previous reports indicating that less acidic environments elicited a lower selectivity towards maleic acid, but increased selectivity towards 2(3*H*)-furanone (**3**) and subsequently succinic acid.[10,14,24] Overall, the influx of labile products formed by an initial Baeyer-Villiger oxidation into different furanones is governed by the Brønsted acidity of the reaction medium and accounts for the selectivity towards maleic acid under highly acidic conditions. These reactivity trends can be ascribed to more avid reactions of protonated furan rings with nucleophilic oxidant, and to the unsurprising faster hydrolysis of cyclic species in the presence of Brønsted acidity.

To further confirm the observed selectivity towards diacids, we decided to conduct an end-point study (24-hour reactions) at different concentrations of formic acid (Figure 9). Unsurprisingly, relative yields of maleic acid appeared to increase with increased concentration of formic acid. The relative yield of succinic acid was found to decrease with increased acid concentration, consistent with expectations. More surprising was the formation of malonic acid (**11**) as the main product for formic acid concentrations of 25-50% (v/v), reaching more than 55% selectivity in 40% (v/v) formic acid. Hence, an intermediate regime of acidity was identified that favors the formation of the C3 diacid **11**. Overall, formic acid concentrations proved to be suitable for favoring accumulation of succinic acid/2(5*H*)-furanone, malonic acid or maleic acid at low, intermediate, and high concentrations, respectively.

CONCLUSION

Here, we provide a diligent mechanistic study of the homogeneous oxidation of furfural in acidic media using advanced NMR-spectroscopic techniques. The use of non-invasive high-resolution spectroscopy in the study of kinetics and mechanisms affords the detection, identification and quantification of transient species by rapid analysis on a single sample. By employing both *in situ* and *ex situ* NMR spectroscopy, we were able to observe and characterize several short-lived intermediates and products by real-time observations, enhancing our understanding of the reaction mechanism (as proposed in Scheme 3). The added sensitivity provided by dDNP NMR clarified initial elusive steps.

We initially identified conditions that allow for the complexity of the acid catalyzed furfural oxidation to be tracked. In this manner, the detection and characterization of novel species, especially hydroperoxide adducts of semialdehyde intermediates, was achieved. The nucleophilicity of hydrogen peroxide and/or performic acid species emerged as a key component in the oxidative conversion of furfural. Using *in situ* ^{13}C NMR spectroscopy, we observed the formation of diacids, including succinic acid (**7**), malic acid (**9**), and malonic acid (**11**), from the hydroperoxide adducts of their semialdehydes (**6**, **8** and **10**). Furthermore, we were able to gain indirect and direct

indication of the formation of the formyl ester of furfural (**2a**) from a peroxy adduct of furfural. These insights were based on the concurrent formation of the furanone **3** and formic acid upon hydrolysis of the formyl ester of furfural **2a**, and by the detection of a novel molecular species in dDNP NMR that was formed later than the hydroperoxy adduct of furfural and prior to the furanone **3**.

The kinetic fitting of the reaction process as tracked by *in situ* ^{13}C NMR spectroscopy was in excellent agreement with the proposed reaction mechanism, considering the complexity of the mechanism. Model and rate constants were derived from conventional NMR spectroscopy under standard conditions, while dDNP NMR observations were used to validate the initial reaction steps. Importantly, our data suggested that the reaction mechanism bifurcates into two separate routes depending on the reaction conditions. The formation of 5-hydroxy-2(5*H*)-furanone (**5**) and subsequently maleic acid (**12**) outcompetes the formation of either of the furanones (2(3*H*)-furanone (**3**) and 2(5*H*)-furanone (**4**)) at low pH values, resulting in a pH-dependent mechanistic outcome. High acid concentrations favor the formation of 5-hydroxy-2(5*H*)-furanone (**5**) and maleic acid (**12**). Lower acid concentrations favored the formation of malonic acid (**11**), while even lower acidity led to a broader distribution of products, including succinic acid (**7**) and 2(5*H*)-furanone (**4**). Overall, the methods and findings of this study encourage the use of experimental studies for rationalizing mechanisms and control of selectivity in complex reaction pathways. We believe that resultant molecular-level insight can be useful in supporting rational catalyst and process design, when transitioning to macroscopic industrial scales.[53–55]

AUTHOR INFORMATION

Corresponding Author

*Sebastian Meier: semei@kemi.dtu.dk

Author Contributions

The manuscript was written through contributions of all authors. All of the authors approved the final version of the manuscript.

Notes

The authors declare no competing financial interest.

ASSOCIATED CONTENT

Supporting Information

The Supporting Information is available free of charge on the ACS Publications website.

PDF with detailed spectroscopic data and kinetic model. Identification of hydroperoxy adducts of furfural and semialdehydes, purification of 2(3H)-furanone, time series using 5-hydroxy-2(5H)-furanone substrate, kinetic fitting, plausible reaction mechanism, and set of ordinary differential equations used for the kinetic model

ACKNOWLEDGEMENT

This research was funded by the Independent Research Fund Denmark (grant 2035-00119B). dDNP data were acquired using instrumentation funded by the Novo Nordisk Foundation (Infrastructure grant NNF19OC0055825). M.G. and A.J. acknowledge funding by the Slovenian Research and Innovation Agency (research projects L2-50050, J4-50148, N2-0242, J1-3020 and N2-0316). The 800 MHz NMR spectra were recorded at the NMR Center DTU, supported by the Villum Foundation. We gratefully acknowledge Christian Oettinger for fruitful discussions aiding the purification of 2(3*H*)-furanone.

REFERENCES

(1) Botti, L.; Kondrat, S. A.; Navar, R.; Padovan, D.; Martinez-Espin, J. S.; Meier, S.; Hammond, C. Solvent-Activated Hafnium-Containing Zeolites Enable Selective and Continuous Glucose–Fructose Isomerisation. *Angew. Chem.* **2020**, *132* (45), 20192–20198. https://doi.org/10.1002/ange.202006718.

(2) Dale, B. E. 'Greening' the Chemical Industry: Research and Development Priorities for Biobased Industrial Products. *J. Chem. Technol. Biotechnol.* **2003**, *78* (10), 1093–1103. https://doi.org/10.1002/jctb.850.

(3) Rass-Hansen, J.; Falsig, H.; Jørgensen, B.; Christensen, C. H. Bioethanol: Fuel or Feedstock? *J. Chem. Technol. Biotechnol.* **2007**, *82* (4), 329–333. https://doi.org/10.1002/jctb.1665.

(4) Centi, G.; Čejka, J. Needs and Gaps for Catalysis in Addressing Transitions in Chemistry and Energy from a Sustainability Perspective. *ChemSusChem* **2019**, *12* (3), 621–632. https://doi.org/10.1002/cssc.201802637.

(5) Okolie, J. A.; Nanda, S.; Dalai, A. K.; Kozinski, J. A. Chemistry and Specialty Industrial Applications of Lignocellulosic Biomass. *Waste Biomass Valor.* **2021**, *12* (5), 2145–2169. https://doi.org/10.1007/s12649-020-01123-0.

(6) *CO2 Emissions in 2022 – Analysis*. IEA. https://www.iea.org/reports/co2-emissions-in-2022 (accessed 2024-10-11).

(7) Shahzadi, T.; Mehmood, S.; Irshad, M.; Anwar, Z.; Afroz, A.; Zeeshan, N.; Rashid, U.; Sughra, K. Advances in Lignocellulosic Biotechnology: A Brief Review on Lignocellulosic Biomass and Cellulases. *ABB* **2014**, *05* (03), 246–251. https://doi.org/10.4236/abb.2014.53031.

(8) Jaswal, A.; Singh, P. P.; Mondal, T. Furfural – a Versatile, Biomass-Derived Platform Chemical for the Production of Renewable Chemicals. *Green Chem.*. **2022**, *24* (2), 510–551. https://doi.org/10.1039/D1GC03278J.

(9) Wu, H.; Song, J.; Liu, H.; Xie, Z.; Xie, C.; Hu, Y.; Huang, X.; Hua, M.; Han, B. An Electrocatalytic Route for Transformation of Biomass-Derived Furfural into 5-Hydroxy-2(5*H*)-Furanone. *Chem. Sci.* **2019**, *10* (17), 4692–4698. https://doi.org/10.1039/C9SC00322C.

(10) Palai, Y. N.; Shrotri, A.; Fukuoka, A. Selective Oxidation of Furfural to Succinic Acid over Lewis Acidic Sn-Beta. *ACS Catal.* **2022**, *12* (6), 3534–3542. https://doi.org/10.1021/acscatal.1c05348.

(11) Zhang, Z.; Huber, G. W. Catalytic Oxidation of Carbohydrates into Organic Acids and Furan Chemicals. *Chem. Soc. Rev.* **2018**, *47* (4), 1351–1390. https://doi.org/10.1039/C7CS00213K.

(12) Choudhary, H.; Nishimura, S.; Ebitani, K. Metal-Free Oxidative Synthesis of Succinic Acid from Biomass-Derived Furan Compounds Using a Solid Acid Catalyst with Hydrogen Peroxide. *Appl. Catal. A: Gen.* **2013**, *458*, 55–62. https://doi.org/10.1016/j.apcata.2013.03.033.

(13) Li, X.; Ho, B.; Lim, D. S. W.; Zhang, Y. Highly Efficient Formic Acid-Mediated Oxidation of Renewable Furfural to Maleic Acid with H_2O_2. *Green Chem.* **2017**, *19* (4), 914–918. https://doi.org/10.1039/C6GC03020C.

(14) Badovskaya, L. A.; Poskonin, V. V. Rearrangements and Tautomeric Transformations of Heterocyclic Compounds in Homogeneous Reaction Systems Furfural–H_2O_2–Solvent. *Russ. J. Gen. Chem.* **2018**, *88* (8), 1568–1579. https://doi.org/10.1134/S1070363218080030.

(15) Badovskaya, L. A.; Poskonin, V. V.; Povarova, L. V. Synthesis of Functional Furan Derivatives by Oxidation of Furans and Formylfurans with Hydrogen Peroxide. *Russ. Chem. Bull.* **2017**, *66* (4), 593–599. https://doi.org/10.1007/s11172-017-1778-8.

(16) Araji, N.; Madjinza, D. D.; Chatel, G.; Moores, A.; Jérôme, F.; De Oliveira Vigier, K. Synthesis of Maleic and Fumaric Acids from Furfural in the Presence of Betaine Hydrochloride and Hydrogen Peroxide. *Green Chem.* **2017**, *19* (1), 98–101. https://doi.org/10.1039/C6GC02620F.

(17) Dalcanale, E.; Montanari, F. Selective Oxidation of Aldehydes to Carboxylic Acids with Sodium Chlorite-Hydrogen Peroxide. *J. Org. Chem.* **1986**, *51* (4), 567–569. https://doi.org/10.1021/jo00354a037.

(18) Gao, X.; Tang, H.; Tong, X.; Zheng, J. Heterogeneous Catalytic Transformation of Biomass-Derived Furans to Selectively Produce C_4 Chemicals with the Simulated Sunlight. *ACS Catal.* **2024**, 16843–16848. https://doi.org/10.1021/acscatal.4c04204.

(19) Lou, Y.; Marinkovic, S.; Estrine, B.; Qiang, W.; Enderlin, G. Oxidation of Furfural and Furan Derivatives to Maleic Acid in the Presence of a Simple Catalyst System Based on Acetic Acid and TS-1 and Hydrogen Peroxide. *ACS Omega* **2020**, *5* (6), 2561–2568. https://doi.org/10.1021/acsomega.9b02141.

(20) Hayes, G.; Laurel, M.; MacKinnon, D.; Zhao, T.; Houck, H. A.; Becer, C. R. Polymers without Petrochemicals: Sustainable Routes to Conventional Monomers. *Chem. Rev.* **2023**, *123* (5), 2609–2734. https://doi.org/10.1021/acs.chemrev.2c00354.

(21) Cross, C. F.; Bevan, E. J.; Heiberg, T. LXXI.—Oxidation of Furfuraldehyde by Hydrogen Peroxide. *J. Chem. Soc., Trans.* **1899**, *75* (0), 747–753. https://doi.org/10.1039/CT8997500747.

(22) Hurd, C. D.; Isenhour, L. L. PENTOSE REACTIONS. I. FURFURAL FORMATION. *J. Am. Chem. Soc.* **1932**, *54* (1), 317–330. https://doi.org/10.1021/ja01340a048.

(23) Alonso-Fagúndez, N.; Agirrezabal-Telleria, I.; Arias, P. L.; Fierro, J. L. G.; Mariscal, R.; Granados, M. L. Aqueous-Phase Catalytic Oxidation of Furfural with H_2O_2: High Yield of Maleic Acid by Using Titanium Silicalite-1. *RSC Adv.* **2014**, *4* (98), 54960–54972. https://doi.org/10.1039/C4RA11563E.

(24) Xiang, X.; Zhang, B.; Ding, G.; Cui, J.; Zheng, H.; Zhu, Y. The Effect of Mg(OH)2 on Furfural Oxidation with H_2O_2. *Catal. Commun.* **2016**, *86*, 41–45. https://doi.org/10.1016/j.catcom.2016.08.013.

(25) Zhang, J.-T.; Wang, H.-Y.; Zhang, X.; Zhang, F.; Guo, Y.-L. Study of Short-Lived and Early Reaction Intermediates in Organocatalytic Asymmetric Amination Reactions by Ion-Mobility Mass Spectrometry. *Catal. Sci. Technol.* **2016**, *6* (17), 6637–6643. https://doi.org/10.1039/C6CY01051B.

(26) Zurlo, E.; Kumar, P.; Meisl, G.; Dear, A. J.; Mondal, D.; Claessens, M. M. A. E.; Knowles, T. P. J.; Huber, M. In Situ Kinetic Measurements of α-Synuclein Aggregation Reveal Large Population of Short-Lived Oligomers. *PLOS ONE* **2021**, *16* (1), e0245548. https://doi.org/10.1371/journal.pone.0245548.

(27) Jensen, P. R.; Knudsen, R. K.; Meier, S. Visualization of Pathway Usage in an Extended Carbohydrate Conversion Network Reveals the Impact of Solvent-Enabled Proton Transfer. *ACS Sus. Chem. Eng.* **2020**, *8* (32), 12270–12276. https://doi.org/10.1021/acssuschemeng.0c04073.

(28) Meier, S. Mechanism and Malleability of Glucose Dehydration to HMF: Entry Points and Water-Induced Diversions. *Catal. Sci. Technol.* **2020**, *10* (6), 1724–1730. https://doi.org/10.1039/C9CY02567G.

(29) Meier, S. Kinetic Variations in Acid-Catalyzed Monosaccharide Conversion. *Catal. Commun.* **2020**, *135*, 105894. https://doi.org/10.1016/j.catcom.2019.105894.

(30) Dusselier, M.; Van Wouwe, P.; de Clippel, F.; Dijkmans, J.; Gammon, D. W.; Sels, B. F. Mechanistic Insight into the Conversion of Tetrose Sugars to Novel α-Hydroxy Acid Platform Molecules. *ChemCatChem* **2013**, *5* (2), 569–575. https://doi.org/10.1002/cctc.201200476.

(31) Dusselier, M.; Van Wouwe, P.; De Smet, S.; De Clercq, R.; Verbelen, L.; Van Puyvelde, P.; Du Prez, F. E.; Sels, B. F. Toward Functional Polyester Building Blocks from Renewable Glycolaldehyde with Sn Cascade Catalysis. *ACS Catal.* **2013**, *3* (8), 1786–1800. https://doi.org/10.1021/cs400298n.

(32) Carraher, J. M.; Fleitman, C. N.; Tessonnier, J.-P. Kinetic and Mechanistic Study of Glucose Isomerization Using Homogeneous Organic Brønsted Base Catalysts in Water. *ACS Catal.* **2015**, *5* (6), 3162–3173. https://doi.org/10.1021/acscatal.5b00316.

(33) Zhang, J.; Weitz, E. An *in Situ* NMR Study of the Mechanism for the Catalytic Conversion of Fructose to 5-Hydroxymethylfurfural and Then to Levulinic Acid Using ^{13}C Labeled D -Fructose. *ACS Catal.* **2012**, *2* (6), 1211–1218. https://doi.org/10.1021/cs300045r.

(34) Warthegau, S. S.; Karlsson, M.; Madsen, R.; Jensen, P. R.; Meier, S. Kinetic and Mechanistic Study of Aldose Conversion to Functionalized Furans in Aqueous Solutions. *Catalysts* **2024**, *14* (3), 199. https://doi.org/10.3390/catal14030199.

(35) Amarasekara, A. S.; Williams, L. D.; Ebede, C. C. Mechanism of the Dehydration of D-Fructose to 5-Hydroxymethylfurfural in Dimethyl Sulfoxide at 150°C: An NMR Study. *Carbohydr. Res.* **2008**, *343* (18), 3021–3024. https://doi.org/10.1016/j.carres.2008.09.008.

(36) Jensen, P. R.; Taarning, E.; Meier, S. Probing the Lewis Acid Catalyzed Acyclic Pathway of Carbohydrate Conversion in Methanol by In Situ NMR. *ChemCatChem* **2019**, *11* (20), 5077–5084. https://doi.org/10.1002/cctc.201901241.

(37) Plainchont, B.; Berruyer, P.; Dumez, J.-N.; Jannin, S.; Giraudeau, P. Dynamic Nuclear Polarization Opens New Perspectives for NMR Spectroscopy in Analytical Chemistry. *Anal. Chem.* **2018**, *90* (6), 3639–3650. https://doi.org/10.1021/acs.analchem.7b05236.

(38) Jensen, P. R.; Meier, S. Catalytic Cycle of Carbohydrate Dehydration by Lewis Acids: Structures and Rates from Synergism of Conventional and DNP NMR. *Chem. Commun.* **2020**, *56* (46), 6245–6248. https://doi.org/10.1039/D0CC01756F.

(39) Keshari, K. R.; Wilson, D. M. Chemistry and Biochemistry of ^{13}C Hyperpolarized Magnetic Resonance Using Dynamic Nuclear Polarization. *Chem. Soc. Rev.* **2014**, *43* (5), 1627–1659. https://doi.org/10.1039/C3CS60124B.

(40) Bowen, S.; Hilty, C. Time-Resolved Dynamic Nuclear Polarization Enhanced NMR Spectroscopy. *Angew. Chem. Int. Ed.* **2008**, *47* (28), 5235–5237. https://doi.org/10.1002/anie.200801492.

(41) Taarning, E.; Sádaba, I.; Jensen, P. R.; Meier, S. Discovery and Exploration of the Efficient Acyclic Dehydration of Hexoses in Dimethyl Sulfoxide/Water. *ChemSusChem* **2019**, *12* (23), 5086–5091. https://doi.org/10.1002/cssc.201902322.

(42) Hansen, A. R. E.; Jensen, P. R.; Meier, S. Pathways and Their Usage in the Conversion of Carbohydrates by Aqueous Barium Hydroxide: Insights from Hyperpolarized and Quantitative NMR. *Catal. Sci. Technol.* **2023**, *13* (2), 362–371. https://doi.org/10.1039/D2CY01519F.

(43) Karlsson, M.; Jensen, P. R.; Duus, J. Ø.; Meier, S.; Lerche, M. H. Development of Dissolution DNP-MR Substrates for Metabolic Research. *Appl Magn Reson* **2012**, *43* (1), 223–236. https://doi.org/10.1007/s00723-012-0336-7.

(44) Keshari, K. R.; Wilson, D. M.; Chen, A. P.; Bok, R.; Larson, P. E. Z.; Hu, S.; Criekinge, M. V.; Macdonald, J. M.; Vigneron, D. B.; Kurhanewicz, J. Hyperpolarized [2-13C]-Fructose: A Hemiketal DNP Substrate for In Vivo Metabolic Imaging. *J. Am. Chem. Soc.* **2009**, *131* (48), 17591–17596. https://doi.org/10.1021/ja9049355.

(45) Ardenkjær-Larsen, J. H.; Fridlund, B.; Gram, A.; Hansson, G.; Hansson, L.; Lerche, M. H.; Servin, R.; Thaning, M.; Golman, K. Increase in Signal-to-Noise Ratio of > 10,000 Times in Liquid-State NMR. *Proc. Natl. Acad. Sci.* **2003**, *100* (18), 10158–10163. https://doi.org/10.1073/pnas.1733835100.

(46) Hansen, T.; Vermeeren, P.; Bickelhaupt, F. M.; Hamlin, T. A. Origin of the α-Effect in SN2 Reactions. *Angew. Chem. Int. Ed.* **2021**, *60* (38), 20840–20848. https://doi.org/10.1002/anie.202106053.

(47) Chang, M.; Gabayno, J. L. F.; Ye, R.; Huang, K.-W.; Chang, Y.-J. Mixing Efficiency Enhancing in Micromixer by Controlled

Magnetic Stirring of Fe3O4 Nanomaterial. *Microsyst. Technol.* **2017**, *23* (2), 457–463. https://doi.org/10.1007/s00542-016-3163-1.

(48) An, T.; Yang, H.; Song, W.; Li, G.; Luo, H.; Cooper, W. J. Mechanistic Considerations for the Advanced Oxidation Treatment of Fluoroquinolone Pharmaceutical Compounds Using TiO2 Heterogeneous Catalysis. *J. Phys. Chem. A* **2010**, *114* (7), 2569–2575. https://doi.org/10.1021/jp911349y.

(49) Guan, Y.; Sowndarya, S. V. S.; Gallegos, L. C.; John, P. C. S.; Paton, R. S. Real-Time Prediction of 1H and 13C Chemical Shifts with DFT Accuracy Using a 3D Graph Neural Network. *Chem. Sci.* **2021**, *12* (36), 12012–12026. https://doi.org/10.1039/D1SC03343C.

(50) Palai, Y. N.; Fukuoka, A.; Shrotri, A. Unlocking the Potential of 5-Hydroxy-2(5H)-Furanone as a Platform for Bio-Based Four Carbon Chemicals. *ACS Catal.* **2024**, *14* (4), 2545–2551. https://doi.org/10.1021/acscatal.3c04872.

(51) Boucher, M. M.; Furigay, M. H.; Quach, P. K.; Brindle, C. S. Liquid–Liquid Extraction Protocol for the Removal of Aldehydes and Highly Reactive Ketones from Mixtures. *Org. Process Res. Dev.* **2017**, *21* (9), 1394–1403. https://doi.org/10.1021/acs.oprd.7b00231.

(52) Badovskaya, L. A.; Povarova, L. V. Oxidation of Furans (Review). *Chem. Heterocycl. Comp.* **2009**, *45* (9), 1023–1034. https://doi.org/10.1007/s10593-009-0390-8.

(53) Šivec, R.; Grilc, M.; Huš, M.; Likozar, B. Multiscale Modeling of (Hemi)Cellulose Hydrolysis and Cascade Hydrotreatment of 5-Hydroxymethylfurfural, Furfural, and Levulinic Acid. *Ind. Eng. Chem. Res.* **2019**, *58* (35), 16018–16032. https://doi.org/10.1021/acs.iecr.9b00898.

(54) Chen, W.; Qian, G.; Wan, Y.; Chen, D.; Zhou, X.; Yuan, W.; Duan, X. Mesokinetics as a Tool Bridging the Microscopic-to-Macroscopic Transition to Rationalize Catalyst Design. *Acc. Chem. Res.* **2022**, *55* (22), 3230–3241. https://doi.org/10.1021/acs.accounts.2c00483.

(55) Chen, W.; Fu, W.; Duan, X.; Chen, B.; Qian, G.; Si, R.; Zhou, X.; Yuan, W.; Chen, D. Taming Electrons in Pt/C Catalysts to Boost the Mesokinetics of Hydrogen Production. *Engineering* **2022**, *14*, 124–133. https://doi.org/10.1016/j.eng.2020.11.014.

Furfural, which is easily formed from sugars, is a promising precursor for bio-sourced chemicals. The upgrading of furfural to these chemicals proceeds through controversially debated pathways. The combination of nuclear magnetic resonance spectroscopy, spin hyperpolarization and kinetic modelling clarifies these pathways and their usage.